Active and Reactive Power Control Method for Three-Phase PV Module-Integrated Converter Based on a Single-Stage Inverter

A. Moghadasi, *Student Member, IEEE*, A. Sargolzaei, *Member, IEEE*, M. Moghaddami, *Student Member, IEEE* A. I. Sarwat, *Member, IEEE,* and Kan. Yen, *Senior Member, IEEE*

***Abstract*—The concept of the module-integrated converters (MICs) incorporated in photovoltaic (PV) has recently imbibed a significant attention due to advantages such as low cost of mass production, high efficiency, easier installation, and improved energy harvest. This paper presents the current-source inverter (CSI) with dc voltage boost capability, called single-stage power conversion system, for grid-tied three-phase PV MIC systems. A reliable control system is adopted to modulate the proposed topology in such a way that provides both active and reactive power in order to meet power system needs. To reduce the number of actives switches, the topology utilizes the modified switching pattern based on conventional space vector pulse width modulation (SVPWM) method. It is demonstrated that the injected active and reactive power can be controlled through two modulation indices introduced in the modified SVPWM switching algorithm. The proposed structure is implemented in hardware and experimentally tested with 300-W laboratory prototype. The results verify the desired performance and robustness of the proposed control scheme for exchanging of both active and reactive powers between the PV MIC and the grid within different operating conditions.**

***Index Terms*—Active and reactive control, boost type, current source inverter (CSI), module-integrated converter (MIC), space vector pulse-width-modulation (SVPWM)**

I. Introduction

FORTUNATELY, the goal of reducing greenhouse gas emissions is aligned to a significant extent with the evolution and penetration of renewable energy sources (RES) [1]. The attempts to reduce the continued pollution are promising in view of the recent dramatic increase of installed photovoltaic (PV) capacity, predicted 25% growth over the next 10 years [2].

Power electronic interface circuit as inseparable and costly part for utilizing the PV system is required to guarantee power exchange from the PV source to the grid without violating the grid codes and standards such as CSA-C22.2, UL 1741, IEEE 1547, and IEC 62109-1 [3]. Practically, the grid interactive PV

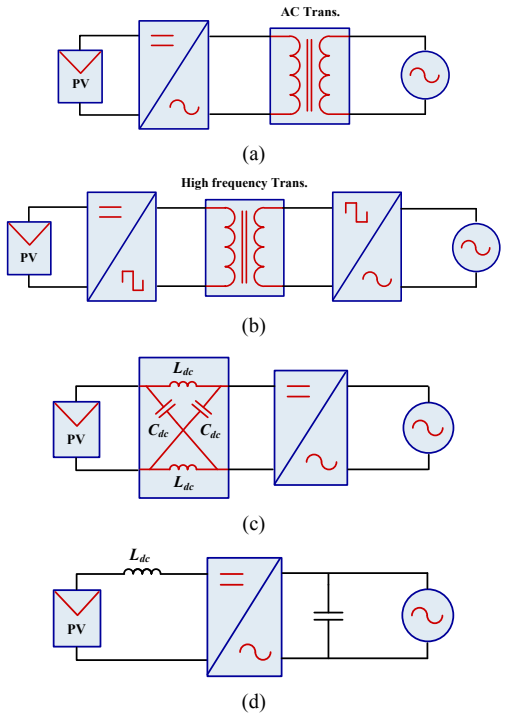

Fig.1. Four options for connecting PV MIC systems. (a) MIC with line-frequency transformer. (b) MIC with high-frequency transformer. (c) Single-stage z-source MIC. (d) Single-stage current source MIC.

structures can be classified into three basic types: centralized inverter, string inverter, and the AC module integrated converter (MIC) (also called microinverter) [4]-[6].

Among these, the MIC is the most recent method of the grid-tied PV systems due to the low cost of mass production, high efficiency, plug and play, and improved energy harvest [7]. With these superior features, MIC concept has become the future trend for PV system development in the market. The commercial PV MIC systems are widely used in single-phase small-scaled distributed PV generation with a power rating range of 150–400W and input dc voltage variation from 20 to 45V. Since the solar panel generates a low-level dc voltage to the MIC, the low PV voltage needs to be boosted to match the utility grid voltage. Considering this issue, several power

Moghadasi, Moghaddami, Sarwat, and Yen are with the Electrical Engineering Department, Florida International University (FIU), Miami 33174, USA, (e-mail:amogh004@fiu.edu).

Sargolzaei is with Department of Electrical Engineering, Florida Polytechnic University, Lakeland, FL.

electronic circuit topologies based on the number of the conversion stages and the design specifications have been studied and presented in the literature [8]-[11]. Figure. 1

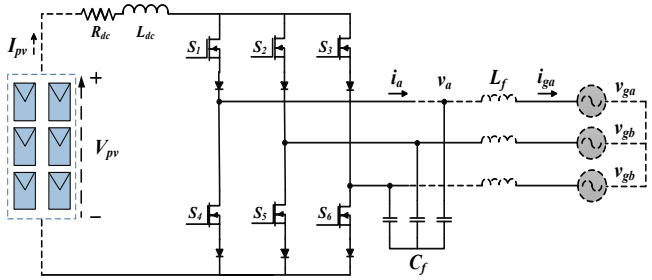

Fig. 2. Three-phase single-stage CSI schematic with MOSFETs for PV MIC system.

summarizes the most commonly used configurations in the presence of PV MIC industry. In Fig. 1(a), a line-frequency transformer is employed to boost the voltage after the voltage source inverter (VSI).

However, a low-power transformer is bulky with load acoustic noise and may not be very efficient. In Fig. 1(b), a high-frequency transformer is introduced to obtain voltage amplifications. Since, high switching frequency is essential to achieve the compact inverter size, the switching loss of the semiconductor devices and the transformer loss are the dominated limitations for efficiency improvement [8]. Figure. 1(c) shows the z-source inverter as another solution which has the capability of boosting and inverting the dc voltage in a single stage with few solid-state switches. However, this topology has relatively high input current ripples, resulting high stresses on the dc-link inductors and capacitors [9]. A single-stage topology based on the current source inverter (CSI) is depicted in Fig 1(d). The CSI can be a viable alternative for other topologies so that circuitry complexity and the overall system losses may be reduced, as discussed in [9], [11]. Also, the CSI has been well documented for high-power drive and rectifier applications, but it is rarely considered in low power ranges (up to 500W) especially in PV MIC industry [12]-[14].

This paper scrutinizes the application of the single-stage CSI topology for the three-phase grid-connected PV MIC system. The proposed structure is implemented in hardware and experimentally tested with 300-W laboratory prototype. While designing a circuit, an effort to minimize the number of switches conducting at any given instant is pursued based on a modified space vector pulse width modulation (SVPWM) method, where possible to reduce the overall system losses and increase the efficiency of the system. A real-time control method with fast transient response and good stability based on the d–q axis principle is also proposed to independently control the active and reactive powers in order to meet power system needs.

II. Circuit Description and Modified Modulation Strategy

The proposed architecture of the three-phase PV MIC based on single-stage CSI is presented in Fig. 2 consisting a bridge with six reverse blocking MOSFET switches (S_1–S_6) in series with a diode, a dc-link inductor L_{dc} as the main energy storage component along with a small amount of the

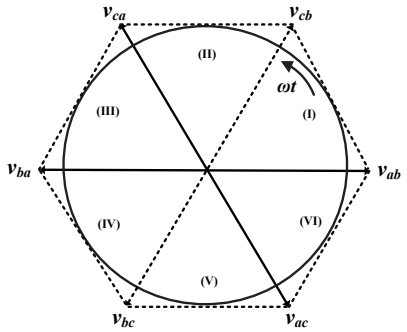

Fig. 3. Six sections in line-to-line voltage phasors.

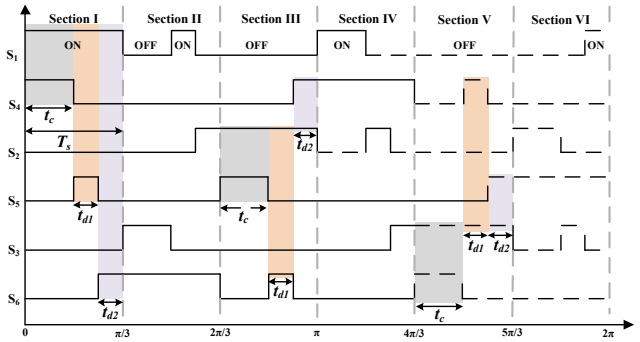

Fig. 4. Switching sequence of all six sections.

resistance R_{dc}, a dc-voltage source V_{pv} representing the output voltage of the PV arrays. The system connected to the three phase grid voltages v_{ga}, v_{gb}, v_{gc} through a high frequency LC filter.

According to the zero-crossing points of grid voltages, there are six Sections (with switching cycle $T_s=\pi/3$) separated by six line-to-line voltage space vectors, v_{ab}, v_{bc}, v_{ca}, v_{ba}, v_{cb}, and v_{ac}, as shown in Fig. 3. Referring to the modified SVPWM modulation strategy discussed in [11], each section is performed by three operating modes and consequently three time intervals. This is accomplished by conducting only two switches at any given instant, one of the upper MOSFETs (S_1, S_3, S_5) and one of the lower MOSFETs (S_4, S_6, S_2) to keep a flow pass for the inductor current. The switching sequence of all six Sections is depicted in Fig. 4, where t_c is the charging time, t_{d1} and t_{d2} are the time intervals of discharging. The relationship of these time intervals gives

$$T_s = t_c + t_{d1} + t_{d2} \tag{1}$$

For instance, Section (I) (0~π/3) can be performed in three time intervals as shown in Fig. 5 and described below.

Interval 1 [$\mathbf{0–t_c}$]*:* S_1 and S_4 are turned on and S_5, S_6 are off. The dc-link inductor is being charged to boost the output voltage, while output currents are supplied by C_{fa}, C_{fb}, C_{fc} (see Fig. 5(a)).

Interval 2 [$\mathbf{t_c–(t_c+t_{d1})}$]: During this period of time, S_1, S_5 are closed, where the inductor current I_{pv} discharges through C_{fa}, C_{fb}, and the grid v_{ga}, v_{gb} (see Fig. 5(b)).

Interval 3 [$\mathbf{(t_c+t_{d1})– (t_c+t_{d1}+t_{d2})}$]: S_1, S_6 are ON and I_{pv}

declines the through C_{fa}, C_{fc}, and v_{ga}, v_{gc}, whereas i_b is supplied by C_{fb}, C_{fc} (see Fig. 5(c)).

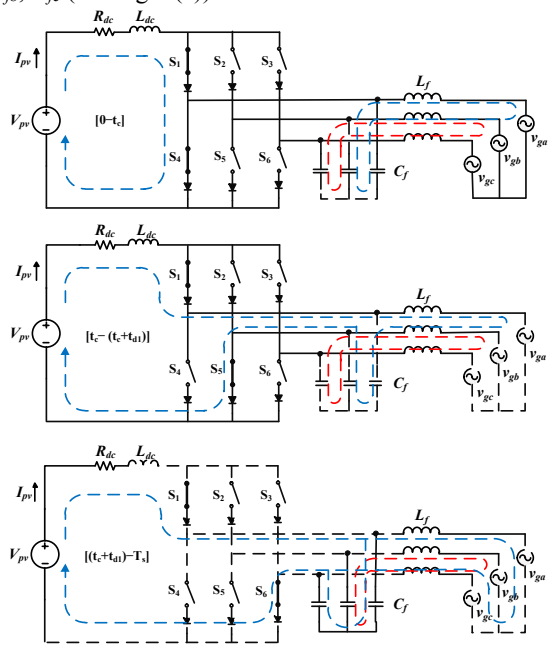

Fig. 5. Three intervals for proposed switching patterns in Section (I) (0~π/3).

In principle, one of the switches is ON for the entire T_s duration in a given Section, while other switches operate at the switching frequency. More details about mathematical formulations for modified SVPWM is represented in [9].

III. Modeling and Control of Three-Phase MCI Based on CSI Topology

A. Average Model of Three-Phase PV MIC

Fig. 6 shows an average equivalent circuit model of single-stage three-phase CSI in the stationary-dq frame. According to Kirchhoff's current and voltage law, the differential equations of the averaged model of the microinverter over switching frequency can be expressed in (2)-(4) by integrating the three time intervals in Section (I) (0~60°).

$$\dot{I}_{dc} = -\frac{R_{dc}}{L_{dc}} i_{pv} - \frac{d_{dq}}{L_{dc}} v_{dq} + \frac{v_{pv}}{L_{dc}} \tag{2}$$

$$\dot{i}_{dq} = \frac{1}{L_f} v_{dq} - \frac{R_f}{L_f} i_{dq} + W i_{dq} \tag{3}$$

$$\dot{v}_{dq} = \frac{d_{dq}}{C_f} i_{pv} - \frac{1}{C_f} i_{dq} - W v_{dq} \tag{4}$$

where, $v_{dq} = \begin{bmatrix} v_d & v_q \end{bmatrix}$, $i_{dq} = \begin{bmatrix} i_d & i_q \end{bmatrix}$ are AC side voltage and current of the inverter, $d_{dq} = \begin{bmatrix} d_d & d_q \end{bmatrix}$ are the discharging duty cycles for the inverter, and $W = \begin{bmatrix} 0 & -\omega_s \\ \omega_s & 0 \end{bmatrix}$

Due to the stationary-dq frame is not a function of time, the averaged model for other sections can be obtained in the same way. In this paper, discharging duty cycles are defined as:

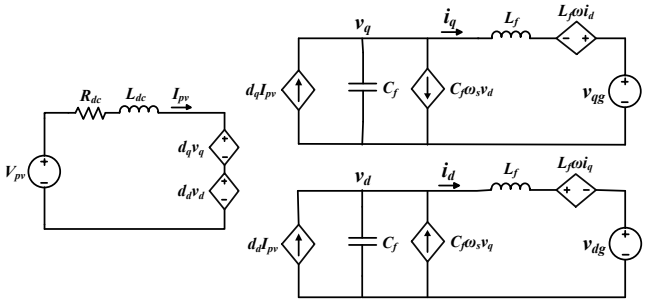

Fig. 6. Average equivalent circuit model of the PV MIC connected to the grid.

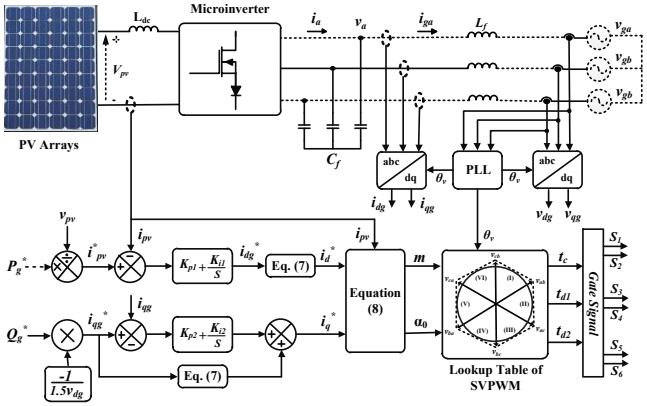

Fig. 7. Block diagram of the proposed control system for CSI-based MIC.

$$\begin{cases} d_d = m\sin(\alpha_0) \\ d_q = m\cos(\alpha_0) \end{cases} \tag{5}$$

where, $0 < m < 1$ is the modulation index, and α_0 is the modulation angle as phase shift with respect to the line-line reference voltage.

B. Proposed Active and Reactive Powers Control of PV MIC

The proposed control block diagram of the PV MIC system shown in Fig. 7. Several *d–q* control algorithms have been reported for inverter power control [15]-[17]. Usually, these methods presented to control the active power based on the maximum power point tracking (MPPT) or follow a fixed active power reference and also control reactive power to provide voltage regulation or track a fixed amount of the reactive power.

In this paper, the proposed power control method is based on voltage-oriented control (VOC), in which the commanded values of the reactive and active power output of the CSI-based MIC system, P_g^* and Q_g^*, can directly be set to the fixed amount with operator. Indeed, the reactive and active powers can be regulated by controlling the modulation index *m* and the modulation angle α_0, properly.

The dc-link current reference i^*_{pv} is acquired by dividing P^* to dc-voltage source V_{pv}, while the dc-link current error is given as the input to a PI controller to generate the *d*-axis grid current command (i^*_{dg}). Also, the q-axis grid current command is determined based on the power-balance assumption:

$$i_{qg}^{*} = \frac{Q_g^{*}}{-1.5 v_{dg}} \tag{6}$$

The reference *d-q* axis inverter current, i^{*}_{d} and i^{*}_{q}, can be calculated by considering the coupled item, *LC* filter, as follows

$$\begin{cases} i_d^{*} = (1-\omega_s^2 L_f C_f) i_{dg}^{*} \\ i_q^{*} = (1-\omega_s^2 L_f C_f) i_{qg}^{*} + \omega_s C_f v_{dg} \end{cases} \tag{7}$$

The current references i^{*}_{d} and i^{*}_{q} in (7) are then applied into the (8) to produce *m* and α_0 and consequently discharging duty cycles d_d and d_q based on (5).

$$\begin{cases} m = \sqrt{i_d^{*2} + i_q^{*2}} / i_{pv} \\ \alpha_0 = \tan^{-1}\left(i_q^{*} / i_d^{*}\right) \end{cases} \tag{8}$$

In order to obtain all these control objectives, CSI-based MIC uses the SVPWM lookup table to engender time intervals of charging and discharging for each section, i.e., t_c, t_{d1}, t_{d2}, while these must follow the angle $\theta_v=\omega t$ calculated from the grid voltages at the same angular speed. Thus, time intervals can be expressed as follows

$$\begin{cases} t_{d1} = m.T_s.\sin(\omega t + \alpha_0) \\ t_{d2} = m.T_s.\cos(\omega t + \alpha_0) \\ t_c = T_s - (t_{d1} + t_{d2}) \end{cases} \tag{9}$$

This switching method offers enough control capabilities for the PV MIC system to keep the suitable steady-state and transient performance.

IV. Experimental Verifications

As shown in Fig. 8, a 300-W grid-connected prototype of the three-phase, single-stage CSI-based MIC was built and tested for real-time active and reactive powers control. A full-bride inverter has been constructed by Fairchild MOSFETs with low R_d (on) and DSEP 30 diodes including the snubber protection circuits. The input voltage of this module is provided by a 50-V power supply connected to the dc-link inductor with L_{dc}=12 mH and R_{dc}=0.4 Ω. The inverter is connected to the grid (3ph, 208 V line to line, 60 Hz) through the ac filter C_f=15 μF and L_f=0.2 mH. The proposed control system is implemented by a dSPACE CLP1104 rapid prototyping board. The MATLAB/Simulink and dSPACE Control Desk are used together to apply the control scheme. The switching frequency was chosen to be 3.0 kHz because of the limitations of dSPACE. The measurements were performed using a LeCroyWaverunner 64XI oscilloscope with a bandwidth of 600 MHz.

Two cases are considered to demonstrate the capability of the proposed control system for real-time active and reactive powers control. It should be noted that the desired value of P_g^{*} is normally dictated by the MPPT algorithm, while the desired value of Q_g^{*} can be chosen according to the power system needs. Figure. 9 and 10 shows dynamic responses of the proposed method to step jumps and falls in the active and reactive power commands. The dynamic response of the

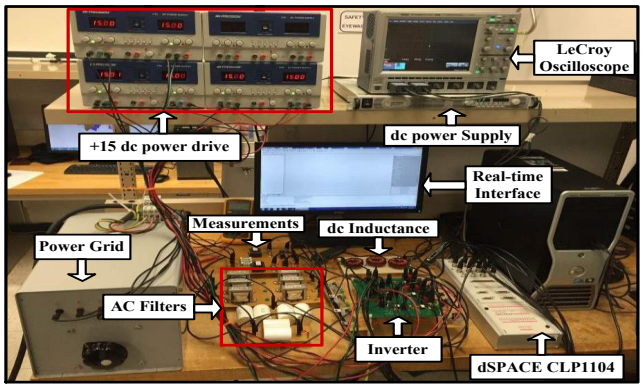

Fig. 8. Layout of experimental setup.

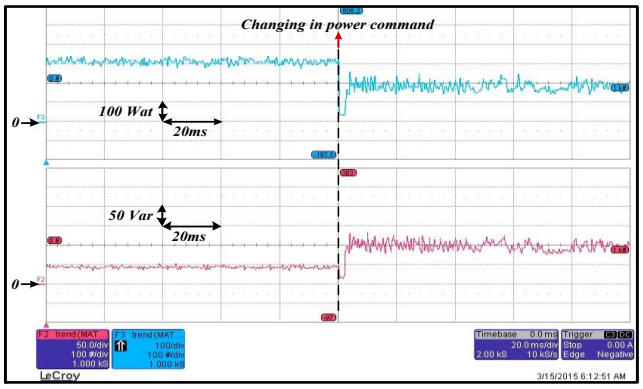

(a)

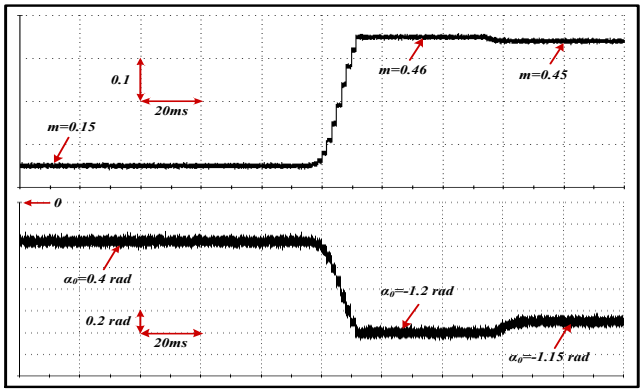

(b)

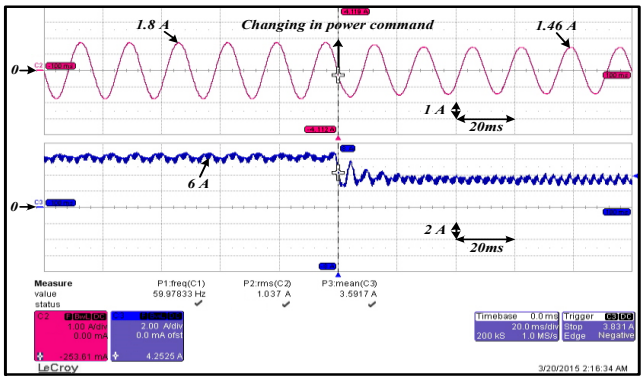

(c)

Fig. 9. Experimental test results for scenario one. (a) Active (100 w/div) and reactive power (50 Var/div). (b) Modulation index m (0.1/div) and modulation angle (Block diagram of α_0 (0.2 rad/div). (c) Phase a current injected to grid (1

A/div) and dc-link current (2 A/div).

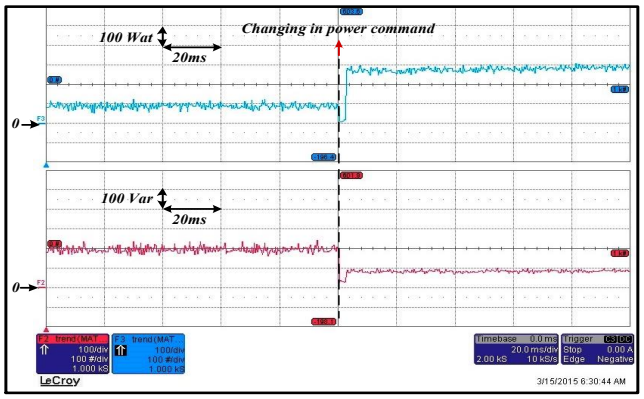

(a)

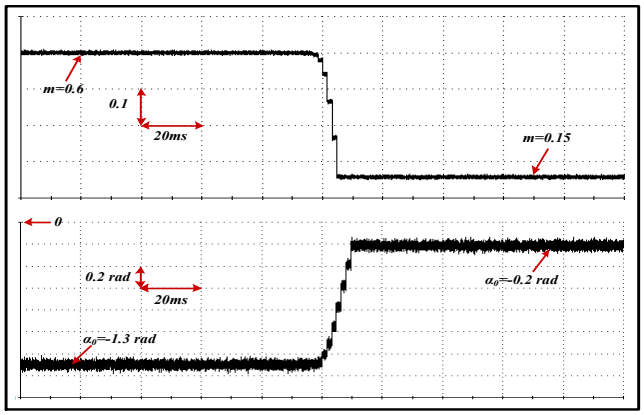

(b)

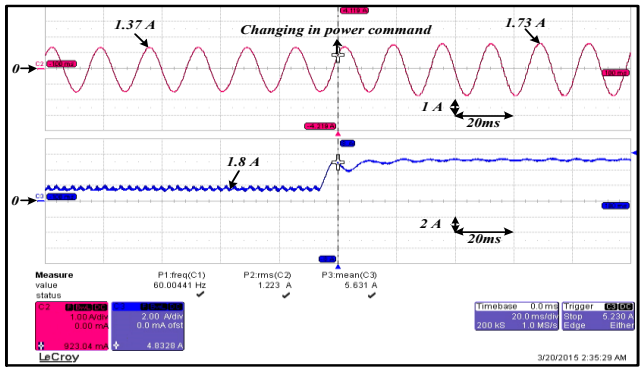

(c)

Fig. 10. Experimental test results for second scenario (a) Active (100 w/div) and reactive power (100 Var/div). (b) Modulation index m (0.1/div) and modulation angle (Block diagram of α_0 (0.2 rad/div). Phase a current injected to grid (1 A/div) and dc-link current (2 A/div).

proposed method is flexibly controlled by the modulation index m and the modulation angle α_0. In case one as indicated in Fig. 9, the active and reactive power commands are set at 300 W and 45 VAR, respectively. Whereas, the control parameters m and α_0 obtained by control system, are kept at the constant values of 0.15 and 0.4 rad, respectively. After 5 cycles, reactive power command jumps from 45 VAR to about 100 VAR and the active power command drops from 300 W to 180 W.

The controller shows very smooth and fast transient response, so that m first went up to 0.46 and then reached 0.45 after three cycles of the power command changing. The modulation angle α_0, also dropped from 0.4 to approximately -1.15 rad (see Fig. 9(b)). Figure. 9(c) also shows a transient response of the phase a current injected to the grid and dc-link current in such a way that provides active power 180 W and reactive power 100 VAR, changing from 1.27 A rms and 6 A dc to 1.03 A rms and 3.6 A dc, respectively.

In the second case shown in Fig. 10, the active power command jumps simultaneously from 90 W to around 280 W and reactive power command drops from 200 VAR to 90 VAR after100 ms. It can be observed that the commands are successfully tracked. In this situation, the control modulations of m and α_0 changed from 0.6 and -1.3 to 0.15 and -0.2 rad, respectively. Fig. 10 (c) displays the phase a current and dc-link inductor current waveforms, increasing to the 1.223 A rms and 5.6 A dc in order to satisfy the desired active and reactive power commands.

V. Conclusion

In this paper, a 300-W three-phase grid-connected CSI-based MIC with single-stage prototype is proposed, constructed, tested. The real-time control method based on the voltage-oriented control (VOC) principle is also proposed and experimentally tested to independently control the active and reactive powers exchanging between the PV and the utility grid in order to meet power system needs. It is demonstrated that the injected active and reactive power can be regulated through modulation index m and the modulation angle α0, introduced into the modified SVPWM switching algorithm. The proposed pattern is based on the SVPWM concept to reduce the overall system losses and increase the efficiency of the system. The experimental results showed fast transient response and good stability which indicate the effectiveness and robustness of the proposed control scheme

References

[1] Dilip A, Marika T. "Sustainable energy for developing countries," S.A.P.I.EN.S [Online], vol. 2, no. 1. pp.1-16, 2009.

[2] European Photovoltaic Industry Association, Global market outlook for photovoltaics until 2016. (2012). [Online]. Available: www.epia.org.

[3] Khajehoddin, S.A.; Karimi-Ghartemani, M.; Bakhshai, A.; Jain, P., "A Power Control Method With Simple Structure and Fast Dynamic Response for Single-Phase Grid-Connected DG Systems," Power Electronics, IEEE Transactions on , vol.28, no.1, pp.221,233, Jan. 2013.

[4] S. B. Kjaer, J. K. Pedersen, and F. Blaabjerg, "A review of single-phase grid-connected inverters for photovoltaic modules," IEEE Trans. Ind. Appl., vol. 41, no. 5, pp. 1292–1306, Sep./Oct. 2005.

[5] L. Quan and P. Wolfs, "A review of the single phase photovoltaic module integrated converter topologies with three different dc link configurations," IEEE Trans. Power Electron., vol. 23, no. 3, pp. 1320–1333, May 2008.

[6] Y. Xue, L. Chang, S. B. Kjær, J. Bordonau, and T. Shimizu, "Topologies of single-phase inverters for small distributed power generators: An overview," IEEE Trans. Power Electron., vol. 19, no. 5, pp. 1305–1314, Sep. 2004.

[7] Yan Zhou; Liming Liu; Hui Li, "A High-Performance Photovoltaic Module-Integrated Converter (MIC) Based on Cascaded Quasi-Z-Source Inverters (qZSI) Using eGaN FETs," IEEE Trans. Power Electron , vol.28, no.6, pp.2727,2738, June 2013.

[8] Quan Li; Wolfs, P., "A Review of the Single Phase Photovoltaic Module Integrated Converter Topologies With Three Different DC Link Configurations," Power Electronics, IEEE Transactions on, vol.23, no.3, pp.1320,1333, May 2008.

[9] Mirafzal, B.; Saghaleini, M.; Kaviani, A.K., "An SVPWM-Based Switching Pattern for Stand-Alone and Grid-Connected Three-Phase

Single-Stage Boost Inverters," Power Electronics, IEEE Transactions on, vol.26, no.4, pp.1102,1111, April 2011.
[10] F. Z. Peng, "Z-source inverter," IEEE Trans. Ind. Appl., vol. 39, no. 2, pp. 504–510, Mar./Apr. 2003.
[11] Y. Chen and K. Smedley, "Three-phase boost-type grid-connected inverter," IEEE Trans. Power Electron., vol. 23, no. 5, pp. 2301–2309, Sep. 2008.
[12] Sahan, B.; Vergara, A.N.; Henze, N.; Engler, A.; Zacharias, P., "A Single-Stage PV Module Integrated Converter Based on a Low-Power Current-Source Inverter," Industrial Electronics, IEEE Transactions on , vol.55, no.7, pp.2602,2609, July 2008.
[13] D. Zmood and D. G. Holmes, "Improved voltage regulation for current-source inverters," IEEE Trans. Ind. Appl., vol. 37, no. 4, pp. 1028–1036, Jul./Aug. 2001.
[14] M. Salo and H. Tuusa, "A vector controlled current-source PWM rectifier with a novel current damping method," IEEE Trans. Power Electron., vol. 15, no. 3, pp. 464–470, May 2000.
[15] F. Katiraei, R. Iravani, N. Hatziargyriou, and A. Dimeas, "Microgrids management," IEEE Power Energy Mag., vol. 6, no. 3, pp. 54–65, May/Jun. 2008.
[16] E. Twining and D. Holmes, "Grid current regulation of a three-phase voltage source inverter with an LCL input filter," IEEE Trans. Power Electron., vol. 18, no. 3, pp. 888–895, May 2003.
[17] F. Blaabjerg, R. Teodorescu, M. Liserre, and A. Timbus, "Overview of control and grid synchronization for distributed power generation systems," IEEE Trans. Ind. Electron., vol. 53, no. 5, pp. 1398–1409, Oct. 2006.